Ocean Sci. Discuss., 12, 2705–2741, 2015
www.ocean-sci-discuss.net/12/2705/2015/
doi:10.5194/osd-12-2705-2015

Ocean Science Discussions

Compensation between meridional flow components of the AMOC at 26° N

E. Frajka-Williams[1], C. S. Meinen[2], W. E. Johns[3], D. A. Smeed[4], A. Duchez[4], A. J. Lawrence[1], D. A. Cuthbertson[1], G. D. McCarthy[4], H. L. Bryden[1], B. I. Moat[4], and D. Rayner[4]

[1]Ocean and Earth Science, University of Southampton, National Oceanography Centre Southampton, SO14 3ZH, UK
[2]Atlantic Oceanographic and Meteorological Laboratory, Physical Oceanography Division, 4301 Rickenbacker Causeway, Miami, FL 33149, USA
[3]University of Miami, Rosentiel School of Marine and Atmospheric Science, 4600 Rickenbacker Causeway, Miami, FL, USA
[4]National Oceanography Centre, Waterfront Campus, European Way, Southampton, SO14 3ZH, UK

Received: 9 October 2015 – Accepted: 2 November 2015 – Published: 13 November 2015

Correspondence to: E. Frajka-Williams (e.frajka-williams@soton.ac.uk)

Published by Copernicus Publications on behalf of the European Geosciences Union.

Abstract

From ten years of observations of the Atlantic meridional overturning circulation at 26° N (MOC, 2004–2014), we revisit the question of flow compensation between components of the circulation. Contrasting with early results from the observations, transport variations of the Florida Current (FC) and upper mid-ocean transports (UMO, top 1000 m east of the Bahamas) are now found to compensate on sub-annual timescales. A deep baroclinic response to wind-forcing (Ekman transport) is also found in the lower North Atlantic Deep Water (LNADW, 3000–5000 m) transport. The observed compensation between the FC and UMO transports is associated with horizontal circulation and means that their individual variability does not project onto the MOC. In contrast, covariability between Ekman and the LNADW transports does contribute to overturning. On longer timescales, the southward UMO transport has continued to strengthen, resulting in a continued decline of the MOC. Most of this interannual variability of the MOC can be traced to changes in isopycnal displacements on the western boundary, within the top 1000 m and below 2000 m. Substantial trends are observed in isopycnal displacements in the deep ocean, underscoring the importance of deep boundary measurements to capture the variability of the Atlantic MOC.

1 Introduction

The Atlantic meridional overturning circulation (MOC) is a key part of the global ocean circulation, redistributing heat and properties around the globe. The continuous daily time-series observations at 26° N are the first of their kind, capturing the transbasin circulation variability on timescales of days to – now – a decade.

From the first year of observations, Cunningham et al. (2007) noted considerable high-frequency variability of the MOC, with values ranging from 5–35 Sv. This exceeds the range of all previous estimates of the MOC strength at 26° N derived from hydrographic sections (Bryden et al., 2005). After three years of data were recovered,

a seasonal cycle of the MOC became apparent (Kanzow et al., 2010), with a maximum in July–November and a minimum in March, and a seasonal range of approximately ±3.5 Sv. This seasonal cycle has been captured by numerical simulations (Xu et al., 2014) and may be explained by variations in wind-forcing on seasonal timescales (Yang, 2015; Duchez et al., 2014). Kanzow et al. (2010) also noted that the components of the MOC (the Florida Current, the interior thermal-wind contribution and the Ekman flow) were largely uncorrelated, suggesting that each contributes variability to the MOC independently. Once the MOC records had stretched to seven years long, striking interannual variability and more recently a declining trend in the MOC were revealed (McCarthy et al., 2012; Smeed et al., 2014). These low frequency changes have consequences for the heat content across the subtropical and tropical North Atlantic (Cunningham et al., 2014; Bryden et al., 2014).

Numerical investigations into the sources of variability to the AMOC interannual variability suggest that much of the variability may be attributable to winds (Roberts et al., 2013; Zhao and Johns, 2014; Yang, 2015). Buoyancy forcing instead affects decadal variations (Polo et al., 2014; Yeager, 2015). An estimate of the MOC from high latitude density anomalies suggests a decline of the MOC (Robson et al., 2014) which is presently observed at 26° N (observed trend of −0.5 Sv, Smeed et al., 2014) though it may not be indicative of a longer-term decline (Roberts et al., 2014). The 26° N array provides an estimate of the MOC, but separating it into components and even depth ranges of anomalies may aid in the identification of physical causes of change (Wunsch and Heimbach, 2013).

In this paper, we introduce the 10 year record of the MOC at 26° N, describing features of the variability in the most recent 18 months and across the ten-year record, and examine more fully the degree of correlation or compensation between MOC components using the longer records. While much of the recent research into Atlantic MOC variability has focused on interannual timescales and longer, here we quantify newly observed compensation between the Florida Current and UMO transports, and covariability between the deep transbasin transports and zonal winds, on sub-annual

timescales. The depth structure and time scales of these variations are explored, illustrating an important role for the western boundary below 1000 m. Lower frequency changes in MOC components, including the continuing trend in the vertical shear of the mid-ocean transport, are also described. Finally, we conclude by discussing the origins of the lower-frequency variability in the 10 year records.

2 Methods

The international 26° N RAPID Climate Change/Meridional overturning circulation and heat flux array (hereafter RAPID 26° N) has provided comprehensive daily measurements of the MOC at 26° N for ten years so far (April 2004–March 2014; Smeed et al., 2015). The MOC is defined as the northward transport above the depth of maximum overturning (roughly 1100 m) across 26° N, and is constructed as the sum of three components: the surface meridional Ekman transport (Ek) estimated from reanalysis winds, the Gulf Stream transport through the Florida Straits – the Florida Current (FC) – measured by a submarine cable (e.g. Meinen et al., 2010), and the upper mid-ocean (UMO) transport, measured by a trans-basin array of current meter and dynamic height moorings between the Bahamas and Africa. The exact number of moorings and instruments has varied over the past decade and more than 20 deployment and recovery cruises. The main western boundary mooring which we used here is called WB2, and typically has 18 MicroCAT (Seabird Electronics, Bellevue, WA) conductivity–temperature–depth instruments. Vertical resolution ranges from 75 m near the surface to 500 m at the bottom. Overall, the accuracy of the MOC transport is estimated to be 1.5 Sv (ten-day values) or 0.9 Sv (annual averages). Full details of the array configuration, transport calculation and associated errors can be found in McCarthy et al. (2015).

Here, we focus on the trans-basin or mid-ocean (MO) transport, from which the UMO is derived. The MO transport is constructed from three parts:

$$\mathrm{MO}(z) = T_{\mathrm{wbw}}(z) + T_{\mathrm{int}}(z) + T_{\mathrm{ext}}(z), \quad (1)$$

where T_{wbw} is the western boundary transport estimated from direct current meter measurements, T_{int} the "internal" transbasin transport and T_{ext} the "external" flow. The western boundary wedge transport, T_{wbw} includes most of the flow associated with the Antilles Current. The "internal" transport, T_{int}, is the baroclinic flow zonally-integrated across the remainder of the ocean interior relative to an assumed level of no motion at 4820 dbar. It is derived from dynamic height moorings near the western and eastern boundaries and over the Mid-Atlantic Ridge. Here we focus on the western and eastern profile contributions to the T_{int}. Using only the western and eastern density contributions to interior transport-per-unit depth, we have that $T_{int}(z)$ relative to the reference level (z_{ref}) is related to density as

$$T_{int}(z) = -\frac{g}{f\rho}\int_{z_{ref}}^{z}\left[\rho_e(z') - \rho_w(z')\right]\,dz', \quad (2)$$

where g is gravitational acceleration, f the Coriolis parameter, and $\rho_e(z)$ and $\rho_w(z)$ the density profiles at the eastern and western boundary, respectively (Rayner et al., 2011).

The "external" flow, T_{ext}, is the (unmeasured) interior barotropic flow that ensures zero mass transport across the section. This component is calculated as a residual of the other components and is applied as a uniformly-distributed (small) velocity across the entire mid-ocean section, which we refer to as "hypsometric compensation". Kanzow et al. (2007) showed that this estimate – derived from mass conservation – was in good agreement with an independent estimate of the mid-ocean barotropic flow derived from bottom pressure gauges deployed across the section.

The MO transport can be further divided into its contributions to the upper and lower branches of the overturning circulation. The UMO is defined as the depth-integral of MO transport between the surface and the time-varying depth of maximum overturning. The mean depth of the maximum overturning is at approximately 1100 m, and in practice there is not much difference between a UMO defined with a time-varying bottom limit of integration vs. a bottom limit fixed at 1100 m. The lower limb of the MOC is made up of southward flowing North Atlantic Deep Water, which is split into contributions associated with upper North Atlantic Deep Water (UNADW; 1100–3000 m) and lower North Atlantic Deep Water (LNADW; 3000–5000 m). The sum of these two transports recovers nearly all the variability of the MOC (r = 0.996, McCarthy et al., 2012). The small difference is equal to the flow between 1100 m and the depth of maximum overturning and a contribution from the hypsometric compensation below 4820 bar.

For the analysis presented here, individual instrument records were two-day low-pass filtered then subsampled onto 12 hourly intervals before computing transports, and then further ten-day low-pass filtered with a 5th-order Butterworth filter. Time series were binned onto a twice-monthly time grid. For lower frequency variations, twice-monthly time series are deseasonalized and filtered with a 1.5 year Tukey filter. Significance and confidence intervals are reported at the 95 % level, unless otherwise indicated. The number of degrees of freedom was calculated using the integral timescale of decorrelation to the first zero crossing (Emery and Thomson, 2004).

For the purpose of calculating isopycnal displacements ζ, in this study, absolute salinities and conservative temperatures on the twice-monthly time grid are used. For reference pressures from the surface to bottom, a mean density profile is calculated within 400 m of the reference pressure, and isopycnal displacements from the mean depth are calculated. Displacements are then mapped back onto the mean depth of each density surface using the time mean profile. The detrended and low-pass filtered time series are processed as above. When a year is denoted 2009/10, it refers to the period 1 April 2009 through 31 March 2010.

3 Ten years of MOC and mid-ocean variability

All of the ten-year time series of transport components at 26° N show high frequency variability (Fig. 1a). In the most recent 18 months, additional features of the time series include a large Ekman transport reversal in March 2013 (similar to the two reversals that

occurred in 2009/10 and 2010/11). During this event, the Ekman transport anomalies exceeded two standard deviations from the mean, with the typically northward-flowing water turned to the south. This reversal was similar in magnitude to the December 2009–March 2010 event, but with shorter duration (Fig. 1a). On several occasions, as during the negative Ekman events in 2005, 2010 and 2013, the FC also showed sharp, short-term reductions in transport. These corresponding anomalies led to sharp reductions – or even brief reversals – of the MOC at these times. The Ekman transport reversals also coincided with reductions of the southward LNADW flow (Fig. 1b). In the most recent 5 years, the LNADW experienced more short periods of reversal (i.e., a northward flow of the net transport below 3000 m) than had been observed in the first 5 years of the record. These high frequency events in the deep flow exhibit fairly weak vertical shear, with maximum anomalies below 3000 m (Fig. 2a).

The MOC exhibits substantial variability at time scales longer than annual (Fig. 3). Interannual variability of the MOC derives primarily from the UMO component, with a negative trend in both over the full 10 year record. The mean and standard deviation of the MOC for the first five years of observations is 18.4 ± 1.3 Sv and the second five years 15.5 ± 1.9 Sv (these values are significantly different, see Table 1). While some of this change is contributed by the 2009/10 dip (McCarthy et al., 2012), the intensification of the southward thermocline flow (UMO) has persisted with the associated weakening of the MOC. The 2012/13 year was the second weakest year of the MOC (14.2 Sv), behind the 2009/10 year (12.8 Sv). In contrast to the 2009/10 year, the weak MOC in 2012/13 had very little contribution from the wind-driven Ekman transport, but instead is associated with a strong southward thermocline flow (UMO).

Transport-per-unit depth anomaly profiles show the depth-structure of mid-ocean transport variations. In the top 1100 m, the southward UMO has intensified (Fig. 2b, shift from red to blue), while below 3000 m the southward LNADW has weakened (shift from blue to red). Previous analyses have shown that variability of the UMO on interannual timescales is primarily governed by changes at the western boundary

(Frajka-Williams, 2015). The amplitude of these changes is larger in the top 1000 m, but anomalies below 1000 m span a large portion of the water column.

4 Correlation between transport components

During the first three years of observations (2004–2007), the components of the MOC (FC, UMO and Ekman) showed little covariability, leading to the conclusion that components contribute their variability independently to the MOC (Kanzow et al., 2010). More recently, sporadic periods of covariability were identified between currents at the western boundary: the FC and Antilles Current (Frajka-Williams et al., 2013). From the ten-year record (2004–2014), we now see correlations emerging between some of the contributing terms, which has implications for how we understand the large-scale circulation at 26° N. Considering the 3 month filtered UMO and FC transport time series (black lines in Fig. 1), anomalies of opposite sign appear to coincide in late 2008, late 2010 and again in late 2012. During the 2010/11 winter, for example, the northward flowing FC weakened by several Sverdrups. At the same time, the southward flowing UMO weakened by nearly 10 Sv. We investigate these apparent compensations (between the UMO and FC, and also between LNADW and wind-driven Ekman flow) more rigorously in the following section.

4.1 UMO and FC transports: Horizontal circulation

The FC carries most of the waters of the Gulf Stream across 26° N. The origins of this water come from the Yucatan Channel and Old Bahama Channel, across complex topography west of the Bahamas (Rousset and Beal, 2014). At similar latitudes, the flow through the Yucatan Channel has been found to compensate flow around Cuba (Lin et al., 2009), while variations in the FC have, at times, shown compensation east of the Bahamas in bottom pressure variations (Bryden et al., 2009) and in top 1000 m velocities (Frajka-Williams et al., 2013).

Here we consider compensation between FC and UMO, the transbasin transport east of the Bahamas. This compensation can be clearly seen by plotting their detrended anomaly time series (Fig. 4a). Certain events stand out, demonstrating almost perfect correspondence between the two time series, with examples including February–May 2007, September 2008–June 2009, August 2010–January 2011 and August 2012–March 2013 (highlighted in the figure). Notably, these episodes of correlation are absent in the first 3 years. The overall correlation between the two records is $r = -0.49$, significant at the 95 % level.

Fluctuations in UMO compensate fluctuations in the FC by similar magnitudes (slope = −0.92, Fig. 4b). When the northward FC transport increases along the western boundary, the southward UMO transport east of the Bahamas intensifies by the same amount. This means that excess northward flow in the boundary current is returned horizontally within the upper mid-ocean circulation rather than by deeper layers in the interior, which would have involved changes in the MOC. The region east of the Bahamas is known to be rich with eddies which may influence the transbasin transports (Wunsch, 2008; Kanzow et al., 2009; Thomas and Zhai, 2013; Clément et al., 2014; Xu et al., 2014), and due to the timescale of observed compensation, we suspect that eddies are involved.

Using the low-pass filtered time series, this high degree of compensation is absent (Fig. 4c and d). Instead, strong interannual variability in the UMO remains (Fig. 4c). By comparison, the low-pass filtered FC shows little interannual variability, consistent with previous work that indicated that the interannual and longer period FC variability is of much smaller amplitude than the sub-annual variability (e.g. DiNezio et al., 2009; Meinen et al., 2010). While the two time series are not significantly correlated ($r = 0.24$), both show a reduction from the first five-year period (April 2004–March 2009) to the latter five-year period (April 2009–March 2014, see also Table 1), with the FC reducing by 0.7 Sv and the UMO by 1.9 Sv. Unlike the compensation at higher frequencies, these changes are both of the same sign (note that the negative of UMO is plotted in Fig. 4a), compounding the effect on the MOC (net reduction of 2.9 Sv).

4.2 LNADW and Ekman transports: Deep wind-driven response

Another – and perhaps more remarkable – correlation that emerges from this analysis is between the deepest limb of the southward mid-ocean transports (LNADW) and the surface meridional Ekman transport (Fig. 5a). Using the detrended anomaly time series, the typically southward LNADW transport can be seen to reduce or even temporarily reverse to northward during strong Ekman transport reversals. (See e.g., events in December 2009–April 2010, November 2010–January 2011, February–March 2013.) The correlation is statistically significant ($r = -0.58$), and can be seen to occur throughout much of the record rather than just during the extreme events. In the low-pass filtered data (Fig. 5c and d), the correlation is stronger than for the UMO and FC. However, due to the low number of degrees of freedom for the low-pass filtered time series (ndof = 5), it is not significant.

As with the FC and UMO compensation, magnitudes of fluctuations between Ekman and LNADW match (slope = −0.84, with Ekman anomalies of 1 Sv corresponding to a 0.84 Sv change in the LNADW). Unlike for the FC and UMO, however, the correlation between the LNADW and Ekman at higher frequencies projects onto the MOC rather than cancelling. This is consistent with expectations that the high frequency, wind-driven variability of Ekman transport results in an overturning, albeit a shallow one between the surface Ekman transport and return flow below (Jayne and Marotzke, 2001; Killworth, 2008). Variations in Ekman or FC project directly on the mid-ocean transport (through the T_{ext} term in 2), and bottom pressure records at the western boundary also covary with Ekman anomalies (McCarthy et al., 2012). However, we will show that the covariations between FC, Ekman and mid-ocean transports are not limited to the T_{ext} contribution, but are instead associated with density changes at the western boundary.

To identify possible lags between the UMO and FC or Ekman and LNADW, we use the 10 day filtered time series. For both correlations, between the UMO and FC and between the Ekman and LNADW, the timescale of the response is fast (Fig. 6). For

the LNADW and Ekman correlation, a maximum correlation of $r = 0.51$ is found at 1 day lag with Ekman leading. This means that the wind response occurs essentially instantaneously. For the UMO and FC transports, a maximum correlation of $r = 0.46$ is found for UMO leading by 0.5 days. This lead-lag relationship can also be seen by inspecting close-zoomed plots of the time series during large anomalies (Fig. 6e). Due to filtering applied to individual instrument data and transport time series, such a short lag is not statistically meaningful.

5 Depth structure of covariability

The hypsometric compensation term (T_{ext}) is mostly depth-independent, but has a vertical profile that scales with the width of the basin as a function of depth. It is nearly uniform from the surface to about 3500 m, and then decreases gradually to zero at the greatest depths in the basin. If the mid-ocean region had no shear (T_{int}=0) and no flow in the wedge ($T_{wbw} = 0$), the MO transport would still be non-zero through this applied compensation, in order to balance the northward FC and Ekman transport. In the absence of strong variations in T_{int}, we would expect to see anti-correlation between the MO transports (e.g., the UMO and LNADW) and the independently estimated FC and Ekman transports. In this case, the MO transport fluctuations would then have a depth structure approximately matching the hypsometric profile. Instead, the MO transport-per-unit-depth profiles often show deep maxima below 3500 m in anomaly plots (Fig. 2a).

This implies that there are considerable changes in the deep shear integrated across the width of the basin, which are reflected in the T_{int} term. The T_{int} term, in turn, is determined by the isopycnal displacements at the eastern and western boundaries, according to a basin-wide thermal wind balance. In the following, we will use isopycnal displacements at the two basin boundaries to investigate the vertical structure of the variability noted above. In the simplest case of a two-layer fluid, a tilted interface marked by the displacement of the interface at the boundaries will have an associated

geostrophic shear between the layers. The strength of the shear increases with the tilt of the interface so that if the interface were at a constant depth at the eastern boundary, the shear would be controlled by displacements at the western boundary.

While the stratification at 26° N is more continuous, we use displacements at the two basin boundaries to investigate the magnitude of the shear variability and the role of east and west in producing these shear anomalies. Using the time-mean density gradient profile, given by $\overline{N}^2(z) = -(g/\rho)\partial\bar{\rho}/\partial z$, the contribution of heave to transport-per-unit-depth can be estimated from Eq. (2) as

$$\widetilde{T}_{int}(z) = \frac{1}{f}\int_{z_{zref}}^{z} \zeta_e \overline{N_e}^2 - \zeta_w \overline{N_w}^2 \, dz', \tag{3}$$

where $\sim$ distinguishes this portion of T_{int} from the more complete calculation in (2). Here, $\zeta_e(z,t)$ and $\zeta_w(z,t)$ are the isopycnal displacements at the east and west, respectively. From (3), we might expect some correspondence between isopycnal displacements and transports, though transports are the vertically-integrated transport-per-unit-depth.

Comparing the UMO transport with both eastern and western boundary isopycnal displacement time series, we find strong correlations (Fig. 7a). In the west, displacements between 300 and 1200 m are significantly correlated with the UMO time series, with a peak at 820 m. Physical expectations and prior results indicated a role for the displacement of the main thermocline in controlling the UMO transport (Longworth et al., 2011; McCarthy et al., 2012; Duchez et al., 2014). The correlation in the east is of similar absolute amplitude but is spread over a broader depth range (200 to $\sim$ 1800 m deep), consistent with the findings of Chidichimo et al. (2010) that the eastern boundary density variations were coherent down to 1400 m.

The FC is also highly correlated with the western boundary thermocline displacement (Fig. 7a). The sign of the correlation has flipped (consistent with the anti-correlation noted between the FC and UMO). This relationship is statistically signifi-

cant, even though the isotherms covarying with the FC are 150 km away from the FC, east of the Bahamas. As might be expected, there is no statistically significant relationship between the thermocline displacements on the eastern side of the basin and the FC transport. Comparing the time series of western boundary isopycnal displacements at 820 m with the UMO transport (Fig. 8a), we find significant correlation where a 10 m downward displacement of the thermocline corresponds to a 1 Sv increase in the UMO transport (Fig. 8b). Given the one-to-one relationship between the FC and UMO (Fig. 4b), this means that a 10 m thermocline displacement is also associated with a 1 Sv change in the FC.

The correlation between LNADW transport and isopycnal displacements is significant at depth (1500–bottom) on the western boundary only (Fig. 7b). The negative correlation can be readily understood in that a depression of deep isopycnals on the western side of the basin causes larger northward shear below 2000 m. That is to say, a depression of deep isopycnals on the western side of the basin will result in a slowing of the southward LNADW (a northward anomaly) relative to the UNADW layer above it. One remarkable feature of this correlation is that it extends vertically over several thousand meters of water (spanning several moored instruments), so that when water at 3000 m moves upwards, a large segment of the water column above and below is also moving upwards (though with differing magnitudes). In this case, a 42 m downward displacement of the isopycnal at 3140 m results in a 1 Sv reduction in the LNADW transport (Fig. 8d).

Isopycnal displacements in a reduced region (2700–3300 m) at the western boundary are also significantly correlated with the surface Ekman transport (Fig. 7b). Positive (northward) Ekman transport anomalies are associated with upward displacements of the deep isopycnals. This means that when the winds blow along 26° N, the deep ocean responds by heaving upwards or downwards across hundreds of meters, with the end result that these isopycnal displacements at the western boundary change the basin-wide tilt and thus the vertical shear in meridional transports. Just 40 km offshore (25 km further offshore than the western boundary) at the WB3 mooring, isopycnal displacements are still significantly correlated with LNADW transports, albeit more weakly ($|r| \leq 0.5$, not shown). Ekman transports are no longer correlated with displacements. At the WB5 mooring, 500 km offshore, there is no relationship between isopycnal displacements and basinwide transport.

6 Timescales of compensation/covariability

One of the key results presented here is that the UMO and FC transports often compensate each other – i.e. their anomalous variability and magnitudes match, but their signs differ – resulting in greatly reduced impact of their individual fluctuations on the total MOC variability. However, this compensation is dependent on timescales. At low-frequencies, the compensation is absent (Fig. 4c), and the large interannual variability and trend in the UMO transport has a strong projection onto the interannual variability and trend of the MOC.

To investigate the covariability for different timescales, we evaluate the coherence calculated using a multitaper spectrum following Percival and Walden (1998) (Fig. 9). The FC and UMO are significantly coherent and out-of-phase (i.e., anti-correlated) at periods less than 1 year. For periods longer than about a year they are no longer coherent. For Ekman and LNADW transports, they are coherent at periods shorter than 900 days (except near 120 days) and also (nearly) out-of-phase. By contrast, there is little coherence between the Ekman and FC time series (Fig. 9, grey).

These results at first appear to contradict Kanzow et al. (2010), who noted from the first 3 years of observations (2004–2007) that there was no compensation between the FC and UMO. Using a cross-wavelet transform (Grinsted et al., 2004), we can examine the temporal shifts in covariability between MOC components (Fig. 10). Since 2007, the FC and UMO covary at annual to sub-annual timescales (consistent with the coherence calculation). Prior to 2007 there is no significant covariation between them (Fig. 10a), consistent with the findings of Kanzow et al. (2010). The cross-wavelet transform of LNADW and Ekman shows that the periods of higher co-variability occur in the latter

half of the 10 year record (Fig. 10b). There also exists some power at annual timescales and higher frequencies (e.g., during the wind-reversal events in 2005, 2009/10 and 2013).

7 Trends in isopycnal displacements and MO transports

The MOC at 26° N has been decreasing in strength, as described in Smeed et al. (2014) and this trend continues through early 2014. This low frequency change is mainly associated with uncompensated changes in the UMO transport (variations at timescales longer than 1 year) and to a lesser degree with a weak reduction in the FC transport (Table 1). From the low-pass filtered transport-per-unit depth profiles (Fig. 2b) we noted that changes are present both above and below the thermocline. Here we investigate how the trends in transport are captured by trends in isopycnal displacements.

At the western boundary, isopycnal displacements below 1000 m are moving downwards (trend at 3140 m is $-6.5 \pm 3.5\,\mathrm{m\,yr^{-1}}$), while above 500 m they are moving upwards (Fig. 11a). At the eastern boundary, trends are near zero except below 4000 m where they are downward. As a result, the east-west slope of isopycnals below 1000 m is decreasing with time. While the largest displacements are seen at depth, stratification is also weaker at depth. From Eq. (3), we see that the effect of isopycnal displacements on transports is modulated by the background stratification. Computing instead the trends in isopycnal displacements scaled by stratification (Fig. 11b), we now see that at the western boundary, the effect of isopycnal displacements below the thermocline is nearly constant, with little effect on the eastern boundary. Scaling by stratification emphasizes the importance of relatively small trends in displacements in the top 1000 m to transport anomalies.

The trend in $\widetilde{T}_{\mathrm{int}}$ from Eq. (3) is shown in Fig. 11c, with a persistent reducing trend in the interior transports associated with heave at the eastern and western boundaries. The magnitude of the trend increases from 0 at the bottom, since it is integrated upwards from the bottom. While the thermocline displacement shows little-to-no trend

(Fig. 11a, the trend on the western boundary at 830 m is $-0.7 \pm 0.9\,\mathrm{m\,yr^{-1}}$), the interior transport has a large negative trend. The large amplitude at the depth of the thermocline results from the accumulation of persistent negative anomalies between the bottom and the thermocline. Above 1000 m, the trend in $\widetilde{T}_{\mathrm{int}}(z)$ is relatively constant and negative.

An overall southward intensification of T_{int}, if unbalanced by other components, would result in an intensification of the southward flow across the section and the 10 year period. To maintain overall mass balance across the section, an opposing trend is required in T_{ext} (Fig. 11d). Trends in the overall mid-ocean transport (MO(z)) include those from $\widetilde{T}_{\mathrm{int}}$ as well as anomalies in the wedge and compensation, due to stratification changes and diabatic changes, and both at the boundaries and mid-Atlantic ridge. The overall amplitude of the trend in MO(z) is weaker than in $\widetilde{T}_{\mathrm{int}}(z)$, but with a greater shear near the surface. The wedge in particular contributes to the shear in the top 1000 m in MO(z) relative to $\widetilde{T}_{\mathrm{int}}$ (not shown).

The trend in MO(z) is negative above ~ 1700 m and positive below. This amounts to a rebalancing of the absolute reference level for T_{int} to account for the changing structure of the interior ocean shear profile. Summing the T_{int} and T_{ext} components results in a northward anomaly below 1700 m (where T_{ext} exceeds anomalies in T_{int}). The vertical structure of these trends explain why the LNADW is seen to be reducing in intensity (less southward than before) while the UMO is increasing in southward intensity. In addition, the depth of the change in the trend (1700 m) is in the middle of the UNADW layer (1100–3000 m) offering an explanation for why no long term trend is apparent in the UNADW transport.

8 Discussion

Here we have identified significant compensation between components of the MOC: e.g., when the FC is stronger northward in the western boundary, the UMO compensates with stronger southward flow between the Bahamas and Canary islands. While

these components are largely independent, they are weakly coupled due to the construction of the MO(z) transports. The T_{ext} term contributes variability to both the UMO and LNADW transport, and would tend to cause an opposite sign anomaly in both the UMO and LNADW in response to anomalies in the FC and Ekman transports.

However, by construction the T_{ext} term is nearly barotropic, and what limited vertical structure it has arises from the vertical profile of section width at 26° N. This means that T_{ext} distributes compensation for the Ekman or FC anomalies across the full water column, with the strongest compensation in the MO(z) term occurring in the top 3500 m and reducing to zero at the bottom. Only a fraction of FC anomalies (order 1/5th) would be projected by T_{ext} onto UMO anomalies, and less than half the magnitude of Ekman anomalies would be contained in the LNADW portion of the T_{ext}. Instead, the observed transport anomalies in UMO and LNADW are indistinguishable in magnitude to the anomalies in FC and Ekman transports. Furthermore, there is no correlation between the Ekman and UNADW transport, which requires a shear between LNADW and UNADW to remove any projected compensation to Ekman. We can see this baroclinic response in the isopycnal displacements measured at the western boundary.

The compensation between the UMO and FC has the appearance of a time-varying horizontal or gyre circulation, but is limited to sub-annual timescales similar to those of eddies identified in Frajka-Williams et al. (2013). In that paper, on some occasions, when a large cyclone (anticyclone) impacted the Bahamas (and T_{wbw} transports), the FC would respond by weakening (strengthening). Sea surface height anomalies originating east of the Bahamas coincided with same sign anomalies along the eastern side of the Florida Straits, resulting in transport anomalies of opposite sign to the west and east of the height anomalies. The new result here is that we use the full UMO rather than just the Antilles Current as in the 2013 paper, and the pattern of anti-correlation has persisted since 2007. Because the co-variability of the FC and UMO transports is accompanied by roughly equal magnitude anomalies, there is a reduced projection of either component on the variability on the overall MOC. This is also consistent with the findings of Clément et al. (2014) who used the RAPID data and sea surface

height anomalies to show that Rossby waves/eddies with a sub-annual timescale do contribute to dynamic height anomalies at the boundary but do not affect the MOC.

The relationship between surface winds and deep isopycnal displacements is harder to understand, and we presently do not have a dynamical explanation for this behavior. Nevertheless, the observations are quite clear: when there is anomalous southward Ekman transport (resulting from westerly winds), isopycnals at ~ 3000 m on the western boundary plunge downwards. From theoretical and numerical model results (Jayne and Marotzke, 2001; Killworth, 2008), it is expected that Ekman transport fluctuations on sub-annual time scales should result in a quasi-instantaneous, and nearly barotropic, compensation in the deep ocean. One might expect that with anomalous southward Ekman transport across the basin, there should be a northward compensation across a broad range of depths, which could also perhaps be spatially distributed. Yeager (2015) showed in a numerical model that Ekman anomalies project strongly onto the barotropic mode promoting wave interactions with deep bathymetry. It is possible that the baroclinic response we observe at 26° N is generated by these barotropic waves interacting with the bathymetry at the western boundary. This is an area for future research – likely requiring numerical modeling to isolate mechanisms and processes.

The observed high-degree of variability on sub-annual timescales of the UMO and LNADW transports may contribute to the apparent absence of meridional coherence between obsevations at 26° N and higher latitudes. Elipot et al. (2013) found large coherence on short time scales at mid-latitudes in the North Atlantic, but between 41 and 26° N, transport anomalies were out-of-phase (Elipot et al., 2014; Mielke et al., 2013). The large fluctuations in LNADW transpot are remarkably well-captured by ocean bottom pressure from the GRACE satellites (Landerer et al., 2015). However, the spatial footprint of detrended monthly anomalies is centered in the western part of the subtropical North Atlantic, suggesting limited meridional coherence. Using satellite altimetry, Frajka-Williams (2015) found that sea surface height anomalies capture the interannual variability and trend of the UMO transport, with a spatial footprint extending over a larger area.

9 Conclusions

The record of basin-wide MOC transport variability at 26° N in the Atlantic is now ten years long. It continues to deliver new insights into the origins of the changing large-scale circulation at 26° N. With the most recent 18 months of observations, the April 2012 to March 2013 year has the second weakest MOC, behind the 2009/10 year. Unlike the 2009/10 year, the reduction in 2012/13 is associated with an enhanced southward UMO and decreased LNADW, with no contribution from anomalous Ekman transport. There were, however, several wind reversal events in the past 18 months, at the end of 2012 and again in March 2013. These events were shorter than the 2009/10 and 2010/11 double dip, though they also resulted in concurrent reductions in the southward LNADW transport.

Using the ten-year record, we now find that on shorter timescales (periods shorter than 1 year), much of the variability of the UMO is compensated by the FC transport variability, particularly in the most recent seven years. On similar timescales (periods shorter than 2 years), the wind-driven variability in the top 100 m (surface meridional Ekman transport) is nearly instantaneously balanced by deep flow in the opposite direction. However, rather than being a simple barotropic response to the winds, the imprint of the winds is baroclinic, with the strongest signature in isopycnal displacements being found east of the Bahamas at 3000 m depth.

There is a key difference between these two compensating transport pairs. Between the FC and UMO, compensated high frequency transport anomalies results in a horizontal circulation anomaly: that is, northward flow in the FC (in the top 700 m) is accompanied by southward flow in the top 1100 m east of the Bahamas. As a consequence, it is unlikely to have a strong heat transport anomaly. By contrast, the southward Ekman anomalies accompanied by northward LNADW anomalies directly projects onto the MOC. During the anomalous periods of exceptionally strong (weak) Ekman transport, the MOC is similarly strong (weak) and we expect the meridional heat transport to vary with the MOC (Johns et al., 2011).

Transport fluctuations on longer timescales present a different story. From the ten-year record, the mid-ocean transports (rather than FC and Ekman) are primarily responsible for the low frequency variability and trend of the overturning. Furthermore, the trend in transport variability is associated with the persistent deepening of isopycnals below the thermocline at the western boundary. These displacements are greatest in the abyss (130 ± 40 m over 10 years at 4500 m) compared to about 60 ± 30 m at mid-depths around 2000 m, though their impact on transports must be scaled by stratification. While we do not investigate here whether the longer-term isopycnal deepening is associated with watermass changes or wind-forcing, a coincident shift towards warmer and fresher waters below 3000 m (Atkinson et al., 2012) hints at the possibility of larger-scale persistent changes to the Atlantic circulation.

Acknowledgements. Data from the RAPID Climate Change (RAPID)/Meridional overturning circulation and heat flux array (MOCHA), Western Boundary Time Series (WBTS) projects are funded by the Natural Environment Research Council (NERC), National Science Foundation (NSF, OCE1332978) and National Oceanic and Atmospheric Administration (NOAA), the Climate Program Office – Climate Observation Division. Data are freely available from www.rapid.ac.uk.

Florida Current transports are funded by the NOAA and are available from www.aoml.noaa.gov/phod/floridacurrent.

Wavelet code provided by A. Grinsted, J. Moore and S. Jevrejeva. Special thanks to the captains, crews and technicians who have been invaluable in the measurement of the MOC at 26° N over the past ten years.

References

Atkinson, C. P., Bryden, H. L., Cunningham, S. A., and King, B. A.: Atlantic transport variability at 25° N in six hydrographic sections, Ocean Sci., 8, 497–523, doi:10.5194/os-8-497-2012, 2012. 2724

Bryden, H. L., Longworth, H. R., and Cunningham, S. A.: Slowing of the Atlantic meridional overturning circulation at 25° N, Nature, 438, 655–657, 2005. 2706

Bryden, H. L., Mujahid, A., Cunningham, S. A., and Kanzow, T.: Adjustment of the basin-scale circulation at 26° N to variations in Gulf Stream, deep western boundary current and Ekman transports as observed by the Rapid array, Ocean Sci., 5, 421–433, doi:10.5194/os-5-421-2009, 2009. 2712

Bryden, H. L., King, B. A., McCarthy, G. D., and McDonagh, E. L.: Impact of a 30 % reduction in Atlantic meridional overturning during 2009–2010, Ocean Sci., 10, 683–691, doi:10.5194/os-10-683-2014, 2014. 2707

Chidichimo, M. P., Kanzow, T., Cunningham, S. A., Johns, W. E., and Marotzke, J.: The contribution of eastern-boundary density variations to the Atlantic meridional overturning circulation at 26.5° N, Ocean Sci., 6, 475–490, doi:10.5194/os-6-475-2010, 2010. 2716

Clément, L., Frajka-Williams, E., Szuts, Z. B., and Cunningham, S. A.: The vertical structure of eddies and Rossby waves and their effect on the Atlantic MOC at 26° N, J. Geophys. Res., 119, 6479–6498, doi:10.1002/2014JC010146, 2014. 2713, 2721

Cunningham, S. A., Kanzow, T., Rayner, D., Baringer, M. O., Johns, W. E., Marotzke, J., Longworth, H. R., Grant, E. M., Hirschi, J. J.-M., Beal, L. M., Meinen, C. S., and Bryden, H. L.: Temporal variability of the Atlantic meridional overturning circulation at 26.5° N, Science, 317, 935–938, 2007. 2706

Cunningham, S. A., Roberts, C., Frajka-Williams, E., Johns, W. E., Hobbs, W., Palmer, M. D., Rayner, D., Smeed, D. A., and McCarthy, G. D.: Atlantic MOC slowdown cooled the subtropical ocean, Geophys. Res. Lett., 40, 6202–6207, doi:10.1002/2013GL058464, 2014. 2707

DiNezio, P. N., Gramer, L. J., Johns, W. E., Meinen, C. S., and Baringer, M. O.: Observed interannual variability of the Florida Current: Wind forcing and the North Atlantic Oscillation, J. Phys. Oceanogr., 39, 721–736, 2009. 2713

Duchez, A., Frajka-Williams, E., Castro, N., Hirschi, J. J.-M., and Coward, A.: Seasonal to interannual variability in density around the Canary Islands and their influence on the AMOC at 26.5° N, J. Geophys. Res., 119, 1843–1860, doi:10.1002/2013JC009416, 2014. 2707, 2716

Elipot, S., Hughes, C., Olhede, S., and Toole, J.: Coherence of western boundary pressure at the RAPID WAVE array: Boundary wave adjustments or deep western boundary current advection?, J. Phys. Oceanogr., 43, 744–765, 2013. 2722

Elipot, S., Frajka-Williams, E., Hughes, C., and Willis, J.: The observed North Atlantic MOC, its meridional coherence and ocean bottom pressure, J. Phys. Oceanogr., 44, 517–537, doi:10.1175/JPO-D-13-026.1, 2014. 2722

Emery, W. J. and Thomson, R. E.: Data Analysis Methods in Physical Oceanography, Elsevier, Amsterdam, the Netherlands, 2nd edn., 2004. 2710

Frajka-Williams, E.: Estimating the Atlantic MOC at 26° N using satellite altimetry and cable measurements, Geophys. Res. Lett., 42, 3458–3464, doi:10.1002/2015GL063220, 2015. 2712, 2722

Frajka-Williams, E., Johns, W. E., Meinen, C. S., Beal, L. M., and Cunningham, S. A.: Eddy impacts on the Florida Current, Geophys. Res. Lett., 40, 349–353, doi:10.1002/grl.50115, 2013. 2712, 2721

Grinsted, A., Moore, J. C., and Jevrejeva, S.: Application of the cross wavelet transform and wavelet coherence to geophysical time series, Nonlin. Processes Geophys., 11, 561–566, doi:10.5194/npg-11-561-2004, 2004. 2718

Jayne, S. R. and Marotzke, J.: The dynamics of ocean heat transport variability, Rev. Geophys., 39, 385–411, 2001. 2714, 2722

Johns, W. E., Baringer, M. O., Beal, L. M., Cunningham, S. A., Kanzow, T., Bryden, H. L., Hirschi, J. J.-M., Marotzke, J., Meinen, C. S., Shaw, B., and Curry, R.: Continuous, array-based estimates of Atlantic Ocean heat transport at 26.5° N, J. Climate, 24, 2429–2449, 2011. 2723

Kanzow, T., Cunningham, S. A., Rayner, D., Hirschi, J. J.-M., Johns, W. E., Baringer, M. O., Bryden, H. L., Beal, L. M., Meinen, C. S., and Marotzke, J.: Observed flow compensation associated with the MOC at 26.5° N in the Atlantic, Science, 317, 938–941, 2007. 2709

Kanzow, T., Johnson, H. L., Marshall, D. P., Cunningham, S. A., Hirschi, J. J.-M., Mujahid, A., Bryden, H. L., and Johns, W. E.: Basinwide Integrated Volume Transports in an Eddy-Filled Ocean, J. Phys. Oceanogr., 39, 3091–3110, 2009. 2713

Kanzow, T., Cunningham, S. A., Johns, W. E., Hirschi, J. J.-M., Marotzke, J., Baringer, M. O., Meinen, C. S., Chidichimo, M. P., Atkinson, C., Beal, L. M., Bryden, H. L., and Collins, J.: Seasonal variability of the Atlantic meridional overturning circulation at 26.5° N, J. Climate, 23, 5678–5698, doi:10.1175/2010JCLI3389.1, 2010. 2707, 2712, 2718

Killworth, P. D.: A simple linear model of the depth dependence of the wind-driven variability of the Meridional Overturning Circulation, J. Phys. Oceanogr., 38, 492–502, 2008. 2714, 2722

Landerer, F. W., Wiese, D. N., Bentel, K., Boening, C., and Watkins, M. M.: North Atlantic meridional overturning circulation variations from GRACE ocean bottom pressure anomalies, Geophys. Res. Lett.,42, 8114–8121, doi:10.1002/2015GL065730, 2015. 2722

Lin, Y., Greatbatch, R. J., and Sheng, J.: A model study of the vertically integrated transport variability through the Yucatan Channel: Role of Loop Current evolution and flow compensation around Cuba, J. Geophys. Res., 114, C08003, doi:10.1029/2008JC005199, 2009. 2712

Longworth, H. R., Bryden, H. L., and Baringer, M. O.: Historical variability in Atlantic meridional baroclinic transport at 26.5° N from boundary dynamic height observations, Deep-Sea Res. Pt. II, 58, 1754–1767, 2011. 2716

McCarthy, G., Frajka-Williams, E., Johns, W. E., Baringer, M. O., Meinen, C. S., Bryden, H. L., Rayner, D., Duchez, A., Roberts, C. D., and Cunningham, S. A.: Observed interannual variability of the Atlantic MOC at 26.5° N, Geophys. Res. Lett., 39, L19609, doi:10.1029/2012GL052933, 2012. 2707, 2710, 2711, 2714, 2716

McCarthy, G. D., Smeed, D. A., Johns, W. E., Frajka-Williams, E., Moat, B. I., Rayner, D., Baringer, M. O., Meinen, C. S., and Bryden, H. L.: Measuring the Atlantic meridional overturning circulation at 26° N, Prog. Oceanogr., 130, 91–111, doi:10.1016/j.pocean.2014.10.006, 2015. 2708

Meinen, C. S., Baringer, M. O., and Garcia, R. F.: Florida Current transport variability: An analysis of annual and longer-period signals, Deep-Sea Res. Pt. I, 57, 835–846, 2010. 2708, 2713

Mielke, C., Frajka-Williams, E., and Baehr, J.: Observed and simulated variability of the AMOC at 26° N and 41° N, Geophys. Res. Lett., 40, 1159–1164, doi:10.1002/grl.50233, 2013. 2722

Percival, D. B. and Walden, A. T.: Spectral Analysis for Physical Applications, Cambridge University Press, Cambridge, UK, 1998. 2718

Polo, I., Robson, J., Sutton, R., and Bamaseda, M.: The importance of wind and buoyancy forcing of the boundary density variations and the geostrophic component of the AMOC at 26° N, J. Phys. Oceanogr., 44, 2387–2408, 2014. 2707

Rayner, D., Hirschi, J. J.-M., Kanzow, T., Johns, W. E., Wright, P. G., Frajka-Williams, E., Bryden, H. L., Meinen, C. S., Baringer, M. O., Marotzke, J., Beal, L. M., and Cunningham, S. A.: Monitoring the Atlantic meridional overturning circulation, Deep-Sea Res. Pt. II, 58, 1744–1753, doi:10.1016/j.dsr2.2010.10.056, 2011. 2709

Roberts, C. D., Waters, J., Peterson, K. A., Palmer, M., McCarthy, G. D., Frajka-Williams, E., Haines, K., Lea, D. J., Martin, M. J., Storkey, D., Blockley, E. W., and Zuo, H.: Atmosphere drives observed interannual variability of the Atlantic meridional overturning circulation at 26.5° N, Geophys. Res. Lett., 40, 1–7, doi:10.1002/grl.50930, 2013. 2707

Roberts, C. D., Jackson, L., and McNeall, D.: Is the 2004–2012 reduction of the Atlantic meridional overturning circulation significant?, Geophys. Res. Lett., 41, 3204–3210, doi:10.1002/2014GL059473, 2014. 2707

Robson, J., Hodson, D., Hawkins, E., and Sutton, R.: Atlantic overturning in decline?, Nat. Geosci., 7, 2–3, doi:10.1038/ngeo2050, 2014. 2707

Rousset, C. and Beal, L. M.: Closing the transport budget of the Florida Straits, Geophys. Res. Lett., 41, 2460–2466, doi:10.1002/2014GL059498, 2014. 2712

Smeed, D. A., McCarthy, G. D., Cunningham, S. A., Frajka-Williams, E., Rayner, D., Johns, W. E., Meinen, C. S., Baringer, M. O., Moat, B. I., Duchez, A., and Bryden, H. L.: Observed decline of the Atlantic meridional overturning circulation 2004–2012, Ocean Sci., 10, 29–38, doi:10.5194/os-10-29-2014, 2014. 2707

Smeed, D. A., McCarthy, G., Rayner, D., Moat, B. I., Johns, W. E., Baringer, M. O., and Meinen, C. S.: Atlantic meridional overturning circulation observed by the RAPID-MOCHA-WBTS (RAPID-Meridional Overturning Circulation and Heatflux Array-Western Boundary Time Series) array at 26° N from 2004 to 2014, available at: https://www.bodc.ac.uk/data/published_data_library/catalogue/10.5285/1a774e53-7383-2e9a-e053-6c86abc0d8c7/, last access: 15 August 2015. 2708

Thomas, M. D. and Zhai, X.: Eddy-induced variability of the meridional overturning circulation in a model of the North Atlantic, Geophys. Res. Lett., 40, 2742–2747, doi:10.1002/grl.50532, 2013. 2713

Wunsch, C.: Mass and volume transport variability in an eddy-filled ocean, Nat. Geosci., 1, 165–168, doi:10.1038/ngeo126, 2008. 2713

Wunsch, C. and Heimbach, P.: Two Decades of the Atlantic Meridional Overturning Circulation: Anatomy, Variations, Extremes, Prediction, and Overcoming Its Limitations, J. Climate, 26, 7167–7186, doi:10.1175/JCLI-D-12-00478.1, 2013. 2707

Xu, X., Chassignet, E. P., Johns, W. E., Schmitz Jr., W. J., and Metzger, E. J.: Intraseasonal to interannual variability of the Atlantic meridional overturning circulation from eddy-resolving simulations and observations, J. Geophys. Res., 119, 5140–5159, doi:10.1002/2014JC009994, 2014. 2707, 2713

Yang, J.: Local and remote wind stress forcing of the seasonal variability of the Atlantic Meridional Overturning Circulation (AMOC) transport at 26.5° N, J. Geophys. Res., 120, 2488–2503, doi:10.1002/2014JC010317, 2015. 2707

Yeager, S.: Topographic coupling of the Atlantic overturning and gyre circulations, J. Phys. Oceanogr., 45, 1258–1284, doi:10.1175/JPO-D-14-0100.1, 2015. 2707, 2722

Zhao, J. and Johns, W.: Wind-forced interannual variability of the Atlantic Meridional Overturning Circulation at 26.5° N, J. Geophys. Res., 119, 2403–2419, doi:10.1002/2013JC009407, 2014. 2707

Table 1. Mean ± standard deviation of transports for the first five years and latter five years, where years run from 1 April–31 March. Standard deviations are calculated on the annual averages. Statistically significant changes to the mean are indicated by bold, based on two-tailed *t* tests.

Component	2004–2009 [Sv]	2009–2014 [Sv]	Change [Sv]
FC	31.7 ± 0.2	31.0 ± 0.3	**−0.7**
Ekman	3.7 ± 0.4	3.4 ± 1.0	−0.3
UMO	−17.0 ± 1.2	−18.8 ± 1.0	**−1.9**
MOC	18.4 ± 1.3	15.5 ± 1.9	**−2.9**
UNADW	−12.0 ± 0.3	−11.8 ± 0.7	0.2
LNADW	−7.1 ± 0.9	−4.7 ± 1.5	**2.3**

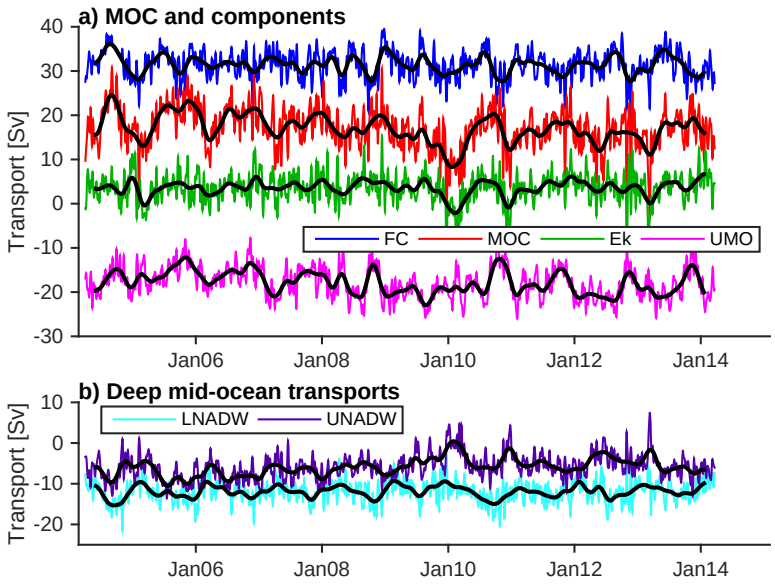

Figure 1. (a) Ten-day (colors) and three month low-pass (black) time series of FC transport (blue), Ekman transport (green), upper mid-ocean transport (magenta) and overturning transport (red). **(b)** Layer transports for UNADW (1100–3000 m, cyan) and LNADW (3000–5000 m, purple). In both panels, the low-pass filter was a 3 month Tukey filter. Transports are positive northwards.

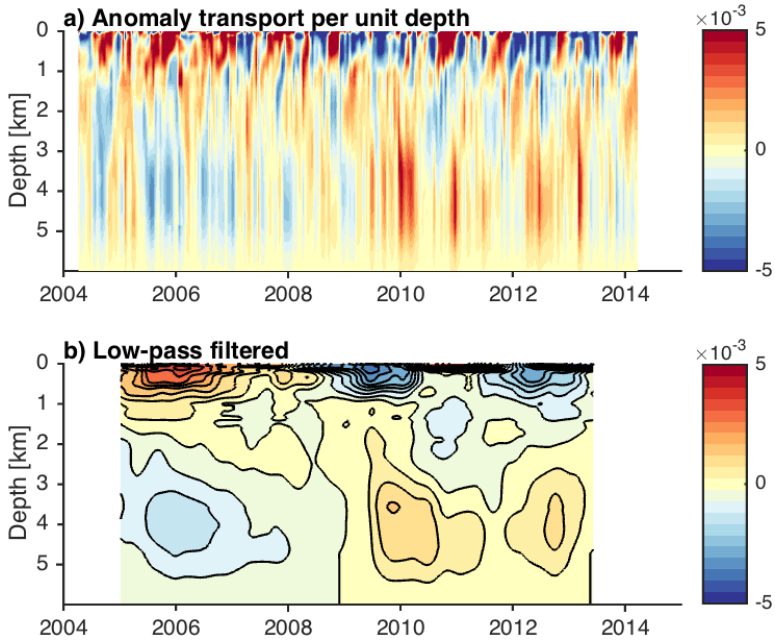

Figure 2. Transport-per-unit-depth anomalies of the mid-ocean transport at 26° N, where the time mean profile has been removed. **(a)** The top panel shows the twice-monthly variability and **(b)** the lower panel is further deseasonalized and filtered with the 1.5 year filter. Red (blue) shows transports which are anomalously northward (southward).

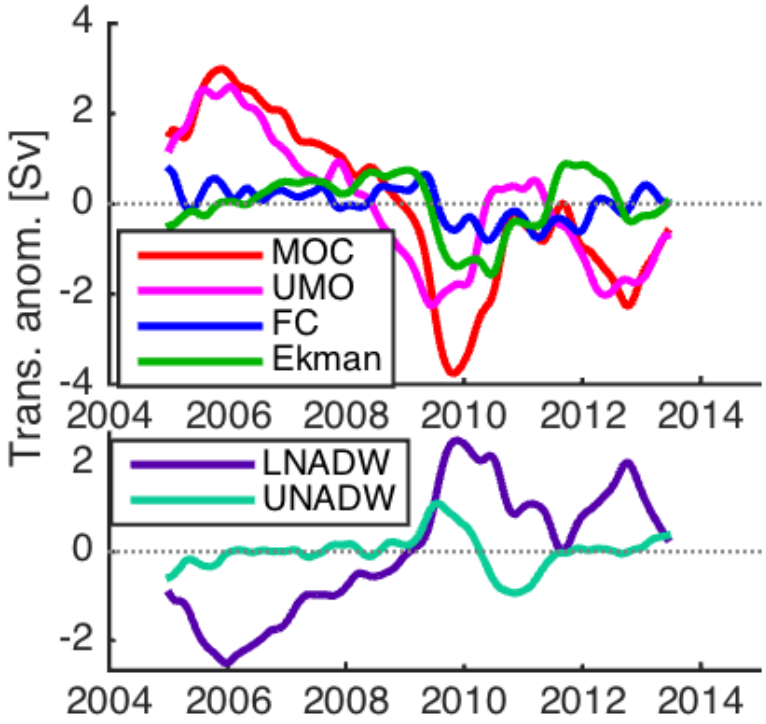

Figure 3. Time series of transport anomaly for MOC and components as in Fig. 1, deseasonalized and low-pass filtered with 1.5 year filter.

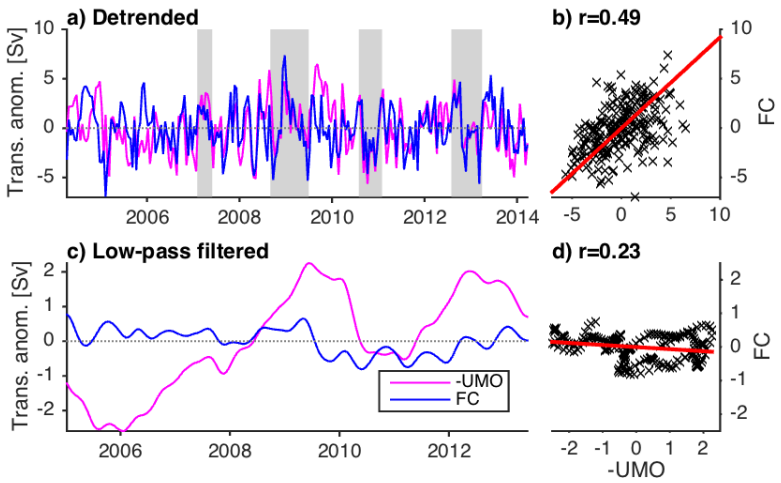

Figure 4. Transport anomaly time series (left column) for the FC (blue) and −UMO (magenta). Zero anomaly is marked with the dashed line. Scatter plots of the same (right column) with correlation coefficients (r) noted. In **(a, b)**, the detrended time series are used. In **(c, d)**, the time series are further deseasonalized and low-pass filtered. The orthogonal regression line is overlaid on the scatter plots. Grey bars highlight periods noted in the text.

Discussion Paper | Discussion Paper | Discussion Paper | Discussion Paper |

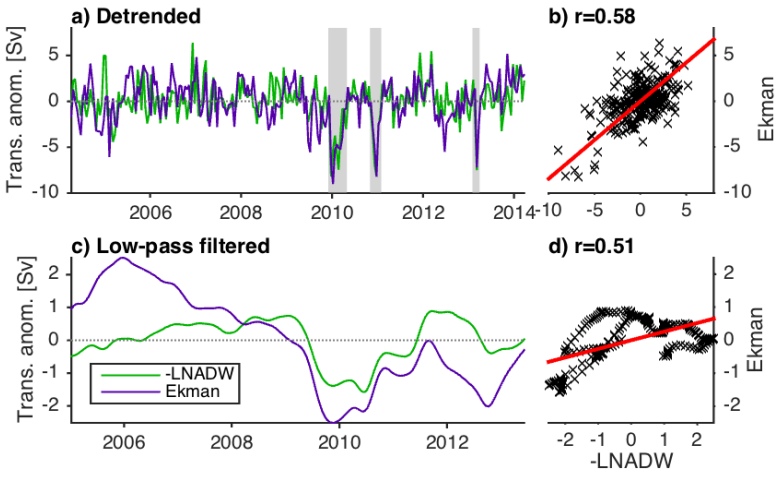

Figure 5. As Fig. 4 but for the Ekman and −LNADW transport anomaly time series.

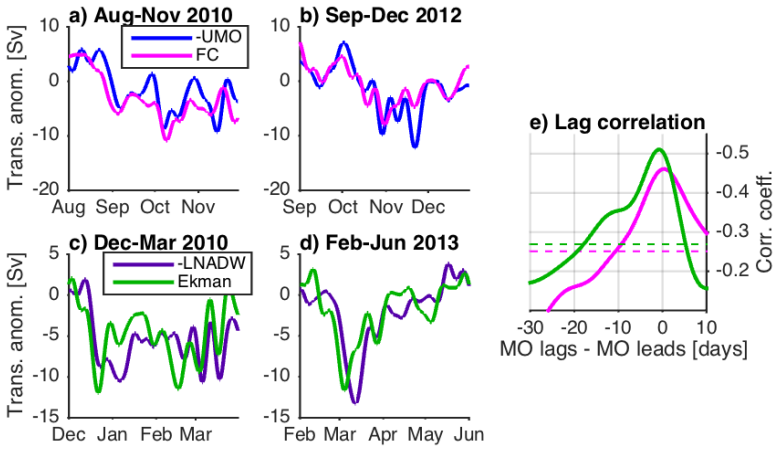

Figure 6. Ten-day filtered transport anomaly time series of UMO and FC **(a, b)** and LNADW and Ekman **(c, d)**. Time ranges have been chosen to correspond to large anomalies in both time series, to visualize possible lags. **(e)** Lag correlation between ten-day filtered UMO and FC (magenta) and Ekman and LNADW (green). 95 % significance is marked by the dashed lines, same color.

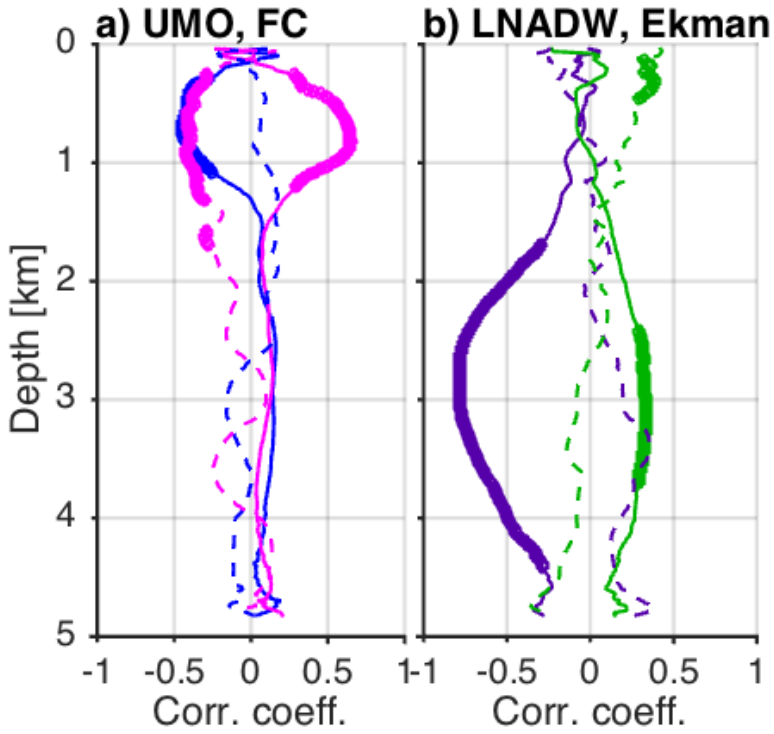

Figure 7. Correlation between isopycnal displacements at each depth and transport time series, where time series are detrended. **(a)** Correlation between UMO (magenta) and isopycnal displacements at the west (solid) and east (dashed), and between FC (blue) and isopycnal displacements at the west (solid) and east (dashed). Significant correlations are indicated by the thicker line. **(b)** The same, but for LNADW (purple) and Ekman (green).

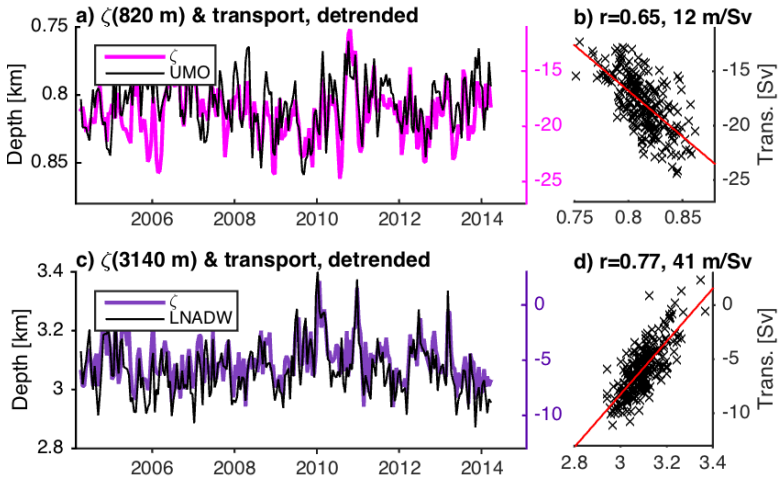

Figure 8. Time series of detrended transports and isopycnal depths. **(a)** UMO transport (magenta) and the depth of the density surface with mean position at 820 m (highest correlation with UMO) at the west. **(c)** LNADW transport (purple) and the depth of the density surface with highest correlation (at 3140 m). Scatter plots are shown in **(b, d)**, where the least squares linear regression is overlaid.

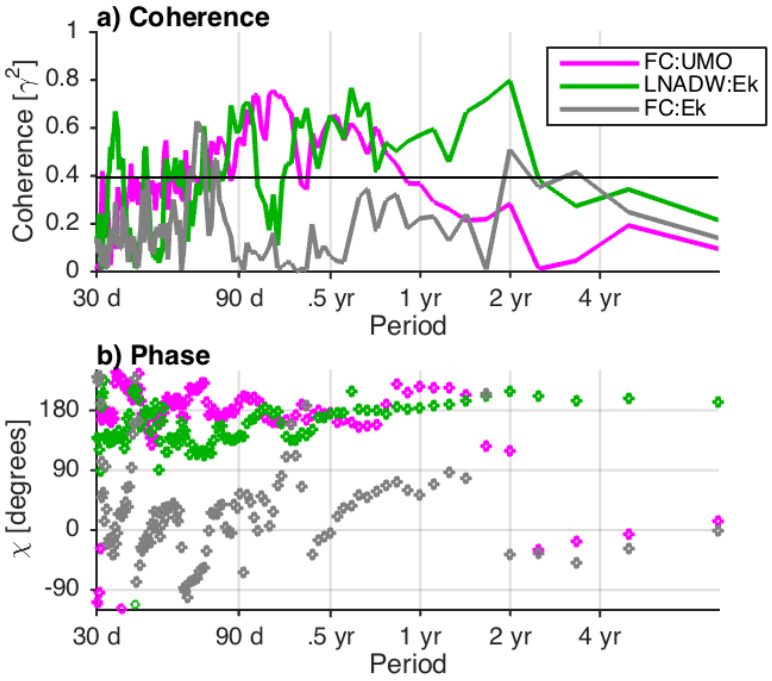

Figure 9. Coherence between MOC components: UMO and FC (magenta), LNADW and Ekman (purple) and FC and Ekman (grey), where time series are 10 day filtered. The top panel shows coherence, where significance is delimited by the black horizontal line. The lower panel shows the phase relationship at each period in degrees.

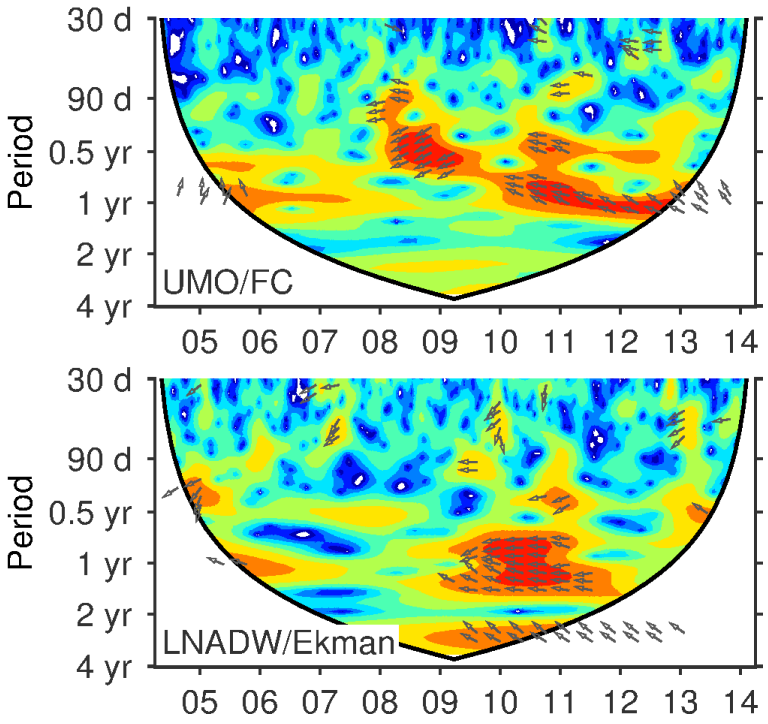

Figure 10. (a) Cross wavelet transform between the FC and UMO shows high power (red) with a fixed phase-relationship since 2007 at periods between 60–400 days. **(b)** Cross wavelet transform between Ekman and LNADW shows high power primarily at annual periods during the 2009–2010 events, as well as sub-annual from 50–150 days in 2005, 2011, and 2013 (Arrows pointing to the left indicate out-of-phase relationship or anti-correlation. Deviations from 180° indicate a lag or phase shift.)

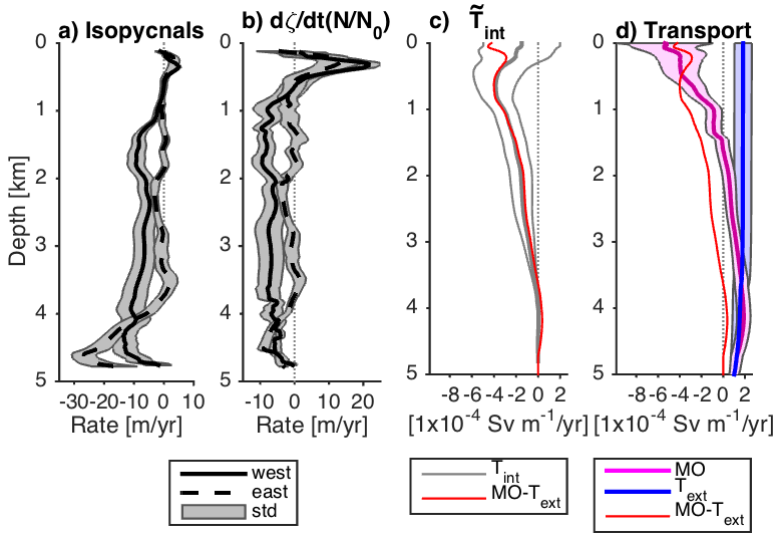

Figure 11. Trend in isopycnal displacements and transports. **(a)** Trend in isopycnal displacements at the western and eastern boundaries, where a negative (positive) trend indicates downward (upward) movement of isopycnals. The solid (dashed) line is for displacements at the west (east). **(b)** Trend in displacements scaled by buoyancy frequency with $N_0 = 1 \times 10^{-3}\,\mathrm{s}^{-1}$. **(c)** Trend in $\widetilde{T}_{\mathrm{int}}$ from Eq. (2). The red line is the trend in MO(z) – T_{ext}. **(d)** Trends in transport-per-unit-depth of mid-ocean (MO(z)) in magenta, T_{ext} in blue. All time series were twice-monthly. Confidence intervals on the trends are shaded. The dotted line shows a zero trend.